Controlling selective nucleation and growth of dysprosium islands on graphene by metal intercalation

Minsung Kim,[1] Myron Hupalo,[1] Michael C. Tringides,[1,2] Patricia A. Thiel,[1,3,*] Kai-Ming Ho,[1,2] and Cai-Zhuang Wang[1,2,†]

[1]*Ames Laboratory, U.S. Department of Energy, Iowa State University, Ames, Iowa 50011, USA*

[2]*Department of Physics and Astronomy, Iowa State University, Ames, Iowa 50011, USA*

[3]*Department of Chemistry and Department of Materials Science and Engineering, Iowa State University, Ames, Iowa 50011, USA*

(Received 23 June 2022; accepted 19 August 2022; published 8 September 2022)

Metal intercalation is an effective method to modify the physical and chemical properties of low-dimensional systems such as epitaxial graphene. Here, we show that the nucleation and growth of metal nanostructures on epitaxial graphene on SiC(0001) can be dramatically changed by metal intercalation. Using scanning tunneling microscopy experiments, we demonstrate that dysprosium (Dy) metal islands are selectively nucleated on the area with Dy intercalation under both graphene and carbon buffer layers, while the adjacent area with only buffer layer intercalated remains relatively bare. Using first-principles calculations based on density functional theory, we show that adsorption of Dy adatom on the preferred nucleation area is energetically more favorable than on other areas. Moreover, changes in the electronic structure and the interlayer spacing upon Dy intercalation obtained from our calculations are also consistent with experimental observations. Our results indicate that metal intercalation is a promising way to manipulate the interaction between graphene and deposited adatoms.

DOI: 10.1103/PhysRevMaterials.6.094003

I. INTRODUCTION

Promising graphene applications, e.g., good metal contacts for device circuits, high density magnetic nanoislands for computer memories, or stable nanoparticles for enhanced catalytic activities, require the ability to control the deposition and growth morphology of metals deposited on graphene surface [1,2]. Recent experiments show that metal intercalation [3–11] provides a way to effectively modify the properties of graphene and tune adatom-graphene interactions. It has been shown that adsorption of metal atoms can be manipulated by the intercalation of metallic layers between graphene and the supporting substrate [7,8]. For example, by preparing a graphene sample on Ir(111) such that Eu (or Cs) intercalated and nonintercalated regions coexist, the nucleation of additional Eu (or Cs) is concentrated on top of the pristine areas whereas the island density on the intercalated regions is essentially zero. Such strong selectivity for nucleation on pristine graphene has been attributed to the adsorption energy difference and the different doping levels between the intercalated and the pristine areas [8].

In this paper, we show that rare earths (REs) can also be intercalated underneath epitaxial graphene supported on SiC (0001) to realize the selective island nucleation and growth. Intercalation of Dy under the carbon buffer layer [we refer to this as single-layer (SL) intercalation] and under both the buffer layer and the single graphene layer [we refer to this as double-layer (DL) intercalation] were observed by heating up to 1600 K after Dy was deposited on graphene at room temperature. Further deposition and nucleation of Dy at 110 K on the intercalated graphene exhibits very interesting morphologies. Dy nucleation on intercalated graphene has been profoundly affected, with preferred Dy nucleation occurring on the DL intercalation rather than on the SL intercalation areas, which is the opposite of the observation in Refs. [7,8] for Eu and Cs adsorption and nucleation on the partially intercalated graphene on Ir(111) substrate. First-principles calculations show that the adsorption energy of Dy on the DL intercalation area is about 52% (or 0.82 eV) larger than that on the SL intercalated area, consistent with our experimental observations.

II. EXPERIMENTAL STUDIES

Experiments were performed using an Omicron variable temperature scanning tunneling microscope (VT STM) with a built-in home-made Dysprosium Knudsen cell thermal evaporator. Such combination provided the possibility for Dy metal deposition on graphene at temperatures as low as 100 K and reproducibly scanning the same area of the sample with ∼10-nm tolerance after several retraction/approach cycles of the STM tip for Dy depositions. Dy flux was calibrated by integration of the volume of the Dy islands in the STM images with an estimated accuracy 5%. As was shown in our previous paper [12], Dy deposits form crystalline islands of fcc structure with (111) orientation after annealing or growth above 650 K. Therefore, a monolayer (ML) was defined by atom density in the close packed (111) plane of Dy fcc or (0001) hcp crystal which is $\sim 9.0\,\text{atoms/nm}^2$.

Prior to the Dy experiment, graphene growth and subsequent sample annealing up to 1600 K were carried out in the attached preparation chamber. High quality uniform and

*Deceased

†wangcz@ameslab.gov

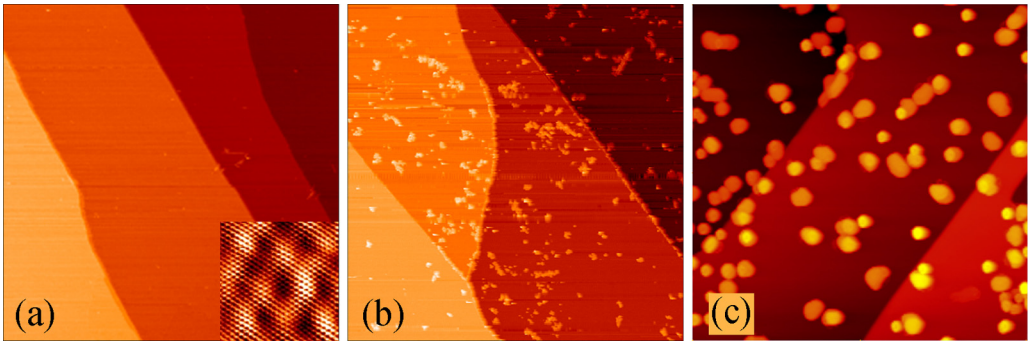

FIG. 1. (a) Initial graphene layer grown on SiC(0001) surface; the inset image with the size about $5.5 \times 5.5\,\mathrm{nm}^2$ shows $(6\sqrt{3} \times 6\sqrt{3})$ corrugation of graphene lattice with atomic resolution. (b) Dy clusters grown at 110 K, $\theta = 0.18$ ML, and scanned at 110 K. (c) Dy crystalline islands formed after annealing to ~900 K for 6 min with $\theta = 1.1$ ML, scanned at room temperature. ~20% of the graphene surface area is covered with islands of average 1.6 nm height. All three images are of $400 \times 400\,\mathrm{nm}^2$.

defect free single layer epitaxial graphene (G1) on Si-terminated SiC(0001) is prepared by thermally annealing 6H-SiC up to ~1450 K for 15 min [13]. Large terraces of G1 with a perfect topography can be seen in Fig. 1(a). The height difference between all adjacent terraces is 0.75 nm which is triple 0.25 nm, the interlayer spacing of SiC(0001), since to prepare one graphene layer three SiC layers are necessary [13,14]. Moreover, Fig. 1(a) indicates that all terraces are equivalent with the same G1 on top of them [i.e., a single layer graphene and a carbon buffer layer (BL) on Si-terminated SiC(0001) substrate].

The inset of Fig. 1(a) shows the atomically resolved structure of the sample. The distinguishing feature here is a long-range $(6\sqrt{3} \times 6\sqrt{3})$ supercell with a 1.8-nm period (of the three 6×6 subcells of the supercell), due to the lattice mismatch between graphene and SiC(0001) surface and the interface structure [13,14]. The magnitude of the corrugation (average roughness) is about 13 pm at a tip-sample voltage larger than 1.5 V, characteristic for the G1 [15]. A separate photoemission experiment confirms that our preparation procedure results in G1 on the SiC(0001) surface [16].

On the top of the G1, Dy atoms are deposited under different conditions. Figure 1(b) shows a STM image of Dy deposit with the coverage $\theta = 0.18$ ML at 110 K and Fig. 1(c) shows the formation of crystalline islands after the Dy deposition with $\theta = 1.1$ ML was annealed to 950 K. Comparison of Figs. 1(b) and 1(c) indicates that Dy nucleation is homogeneous in a wide range of temperatures (1000 K) and coverages ($\theta = 0.2$–1.2 MLs). Small deviations could be caused by kinetic effects due to extra diffusion barriers uphill or downhill at steps separating different terraces.

After the initial Dy deposition on pristine graphene, the sample was annealed up to 1200 K for 5 min. During annealing, part of Dy desorbs but some fraction of Dy intercalates underneath the carbon layers. The sample after Dy intercalation is shown in Fig. 2(a) where a single graphene terrace has been developed into two areas of different heights and with a very wavy boundary, a morphology not commonly observed for the clean graphene. The height histogram of the two areas in the box outlined with a white square in Fig. 2(a) shows that the difference in protrusion heights between the areas is about 0.11 ± 0.01 nm, as one can see from the height histogram plot in Fig. 2(b). From our first-principles calculations as shown later, this height difference is due to two different Dy intercalation structures. In the lower area, only the carbon buffer layer is intercalated (i.e., SL intercalated). In the higher area, both the buffer layer and the graphene layer are intercalated (i.e., DL intercalated).

To prove that the observed protrusions are also related to the electronic structure difference in the two areas due to different intercalation phases, we applied standard scanning tunneling spectroscopy (STS) to measure the dI/dz, i.e., derivative of tunneling current I versus tip-sample separation z, via modulation of z and detecting response of tunneling current I with lock-in amplifier. In a good approximation, for a small tip-sample voltage $V_{\mathrm{t-s}}$, which does not significantly affect the tunneling barrier height ϕ, the tunneling current I is proportional to $V_{\mathrm{t-s}}\exp(-A\phi^{1/2}z)$ where z is the tip-sample separation and ϕ is defined as the average work function of tip and sample $(\phi_{\mathrm{t}} + \phi_s)/2$ [17,18]. The tunneling current modulation signal dI and the tunneling barrier height are related by $\phi^{1/2} \sim d(\ln I)/dz$. Therefore, for two areas with different work functions $\phi_1/\phi_2 = (dI_1/dI_2)^2$, if $\phi_1 - \phi_2 \ll \phi$ and the average tunneling current I is kept constant by the feedback loop during the scan. It should be noted that despite the absolute values of work function being affected by charge density, the charge transfer, as well as the local density of states in different areas of the systems, the *ratio* of work functions depends only on the dI/dz from STS measurement.

Our measurement results plotted in Fig. 3(c) show that the modulated signal dI is 0.93 a.u. for the single-layer intercalated (lower) area verses 0.85 a.u. for the double-layer intercalated (higher) area, indicating that the single-layer intercalated area has a work function about 1.2 times higher than that of the double-layer intercalated area. Noting that the work function of epitaxial graphene on SiC(0001) is about 4.0 eV, we can infer that the work function on the single-layer intercalated area is about 0.8 eV higher than that on the double-layer intercalated area**.** This measurement result is consistent with the Dirac cone shift from our first-principles calculations which will be shown later**.**

We also note that a work function difference between the two areas would also affect the measurement of apparent height difference between the two areas. Scanning at constant tunneling current and voltage requires $\phi^{1/2}\ z$ to remain a constant during the scan. If the scanning is over areas with

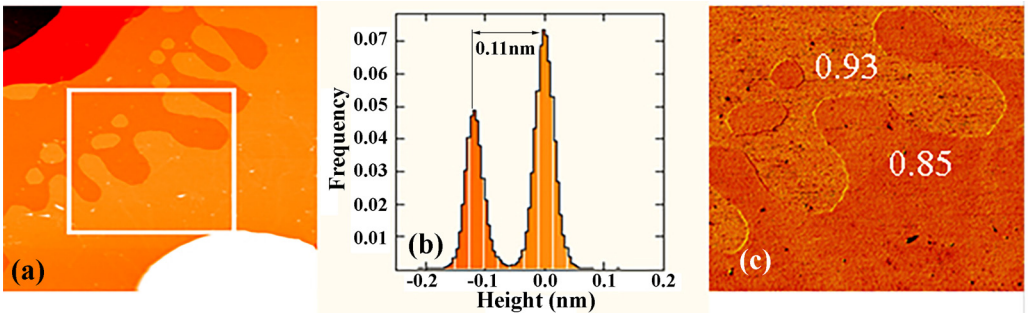

FIG. 2. (a) Topography of Dy-G structure as in Fig. 1(c), annealed at 950 and 1200 K for 5 min each, $500 \times 500\,\mathrm{nm}^2$ area. (b) Height histogram of the area within white square in (a). (c) dI/dz map of the area outlined with the white square in (a). Note that the dI/dz of 0.93 a.u. vs 0.85 a.u. shows the single-layer intercalated area has work function about 1.2 times higher than that of the double-layer intercalated area, consistent with the Dirac cone shift from our first-principles calculations, which will be shown later.

different work functions, we should have $\phi_1^{1/2}\ z_1 = \phi_2^{1/2} z_2$, thus $z_1/z_2 = dI_2/dI_1$. From this follows that the tip approaches closer to the surface region with higher work function and retracts from the areas with lower ϕ. This manifests in the appearance of a small step in a topographical STM image even on a flat surface with different work function ϕ . In our experiment $dI_{\mathrm{low}}/dI_{\mathrm{high}} = 0.93/0.85 = 1.1$. Since under normal operation condition z is in the range 0.2–0.3 nm, the apparent height of the protruded region as shown in Fig. 2(b) should be reduced by 0.02–0.03 nm from 0.11 nm to 0.08–0.09 nm.

Further annealing by short flashing up to 1600 K for 30 sec, the higher the area in Fig. 2 becomes the more compact and the boundary between the low and high areas indicated by the blue dashed line also becomes more straight. We also note that the $(6\sqrt{3} \times 6\sqrt{3})$ corrugation in both low and high areas is not visible, as shown in Fig. 3(b), consistent with our interpretation that both areas are intercalated with Dy. The line scan across the boundary of the two areas [indicated by the green horizontal line in Fig. 3(b)] shows the apparent height difference of about 0.1 nm, as one can see from Fig. 3(c).

After the preparation of the mixed surface with different intercalation areas coexisting, the surface is cooled to 110 K. Then Dy is deposited with small portions at this low temperature as shown in Fig. 4. Clearly the area with 0.1-nm protrusions is more populated with the deposited Dy than the lower area. As the amount of deposited Dy increases, more Dy is found to nucleate on the higher (double-layer intercalated) area as shown in Figs. 4(b)–4(e). The average size of the nucleated islands (forming the shown crowded regions) is larger than 5 nm and 2–3 atomic layers in height. These experiments clearly demonstrate that nucleation and growth of Dy islands on the higher protruding (double-layer intercalated) area is much higher than that on the lower (single-layer intercalated) area.

III. FIRST-PRINCIPLES CALCULATIONS

In order to elucidate the effects of Dy intercalation on the nucleation of Dy on graphene, we perform first-principles calculations to study the adsorption energies of Dy on graphene with SiC substrate. The structure models used in our calculations consist of epitaxial graphene on Si-terminated 6H-SiC(0001) substrate. The substrate was described by two 6H-SiC(0001) layers and a carbon buffer layer. A $2\sqrt{3} \times 2\sqrt{3}R30^\circ$ SiC supercell was adopted on which the 4×4 buffer layer and graphene layer were accommodated, as schematically shown in Fig. 5(a). Due to the limitation of *ab initio* calculation to handle a large number of atoms, the unit cell adopted in our calculations may cause some stress in the system. Under such a lattice mismatch situation, we adjust the size of the unit cell to accommodate the graphene layer in

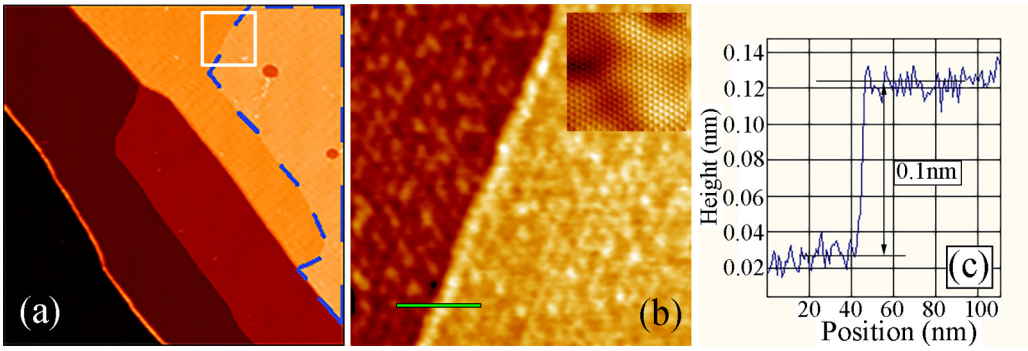

FIG. 3. (a) Morphology of Dy intercalated sample at 1600 K, $250 \times 250\,\mathrm{nm}^2$. Histogram of the area outlined with the white square is similar to Fig. 2(b) and shows height difference 0.1 nm. (b) $40 \times 40\,\mathrm{nm}^2$ area with both lower and higher domain show no periodic $(6\sqrt{3} \times 6\sqrt{3})$ corrugation. $5 \times 5\,\mathrm{nm}^2$ inset at the top right corner of (b) shows atomic resolution of image (b). (c) The green line profile in Fig. 3(b) shows height difference of 0.1 ± 0.01 nm between low and high domains.

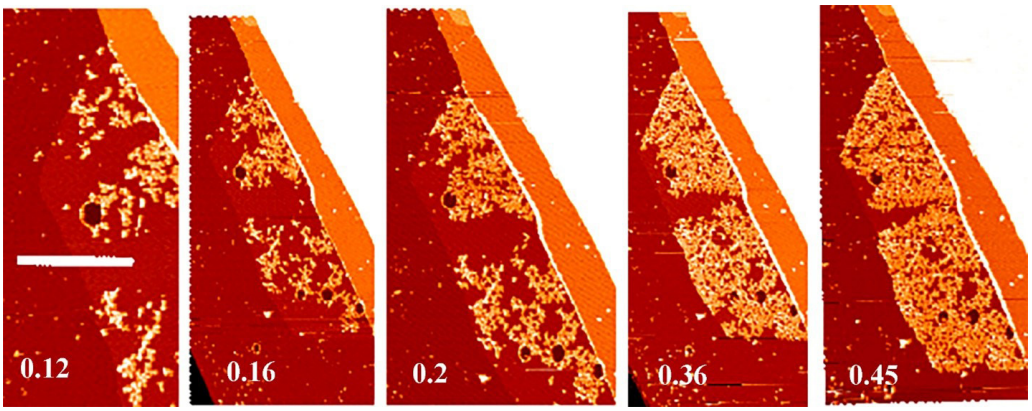

FIG. 4. Sequence of STM scans of the same area during successive deposition of Dy at the flux 0.018 ML/min at 110 K. Dy coverage in monolayers shown at the bottom of subsequent images of approximately the same 280 × 380 nm^2 area. The line scan along the white horizontal line in the leftmost panel shows that the height difference between the two domains is about 0.1 nm, similar to that shown in Fig. 3(c).

its equilibrium lattice constant to minimize the stress effects on graphene. Also, a 2 × 2 intercalation of Dy layer(s) in the supercell (i.e., 4 Dy intercalants in the cell per layer) was assumed. We consider two types of intercalation geometries, i.e., intercalation of Dy atoms between the SiC substrate and the buffer layer (SL intercalation) as shown in Fig. 5(c), and intercalation of Dy atoms under the graphene layer as well as the buffer layer (DL intercalation) as shown in Fig. 5(d).

The first-principles calculations were performed using Vienna *ab initio* simulation package (VASP) [19,20] which is based on density functional theory (DFT). Projector-augmented wave (PAW) potentials [21] were used to describe the interaction between the core and the valence electrons and the wave functions of the valence electrons were expanded using a plane-wave basis set with cutoff energy 400 eV. A 6 × 6 × 1 *k*-point mesh was employed. The Perdew-Burke-Ernzerhof (PBE) exchange-correlation functional [22] was used. We also adopted the DFT-D3 method [23] to include the van der Waals energy. All atoms in the calculation supercells have been relaxed until the force on each atom is less than 0.02 eV/Å, and the criterion for energy convergence in the self-consistent calculation is set to be 10^{-6} eV/atom.

In order to verify that the intercalation structure models used in our calculation is a reasonable choice, we calculated and compared the energy for 2 × 2 Dy on the top of graphene, under the top layer of graphene, and under the buffer layer,

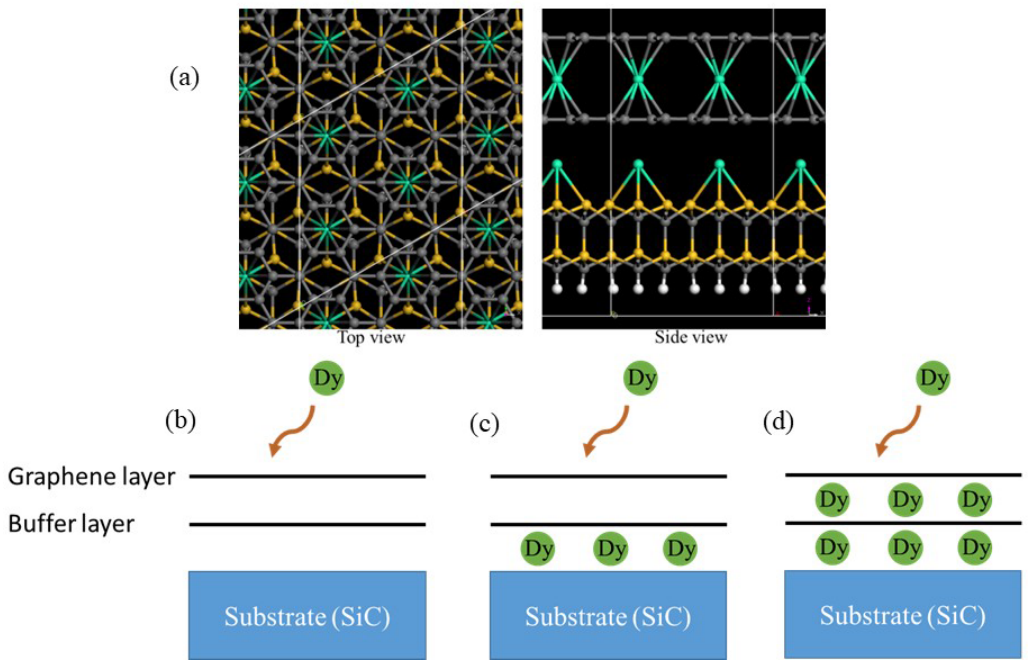

FIG. 5. Atomic structure in DFT calculations. (a) Top view (left) and cross-section view (right) of the atomic configuration of the epitaxial graphene with Dy intercalation. The grey balls are carbon, golden balls are Si, cyan balls are intercalated Dy, and the white balls at the bottom of the SiC substrate are passivated H. (b)–(d) Schematic illustrations for the adsorption on the epitaxial graphene where (b) without intercalation, (c) with Dy intercalation only under the carbon buffer layer (refer to as single layer Dy intercalation), and (d) with Dy intercalation in both upper and lower carbon layers (referred to as double layer Dy intercalation).

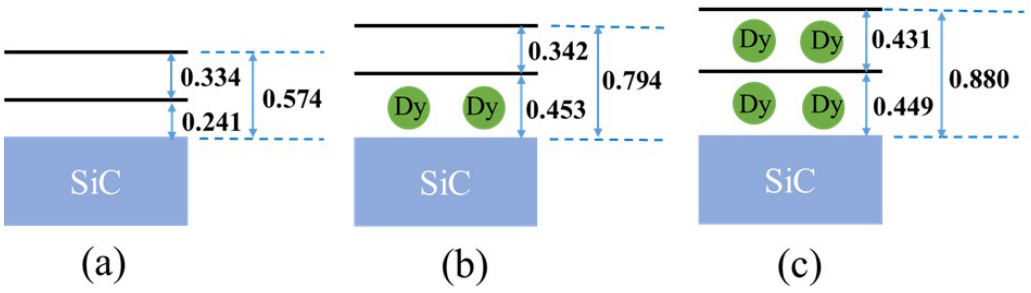

FIG. 6. Interlayer distances in intercalated epitaxial graphene obtained from first-principles calculations. Interlayer distances (in units of nm) among two carbon layers and the outermost Si layer of the substrate are denoted for the epitaxial graphene (a) without intercalation, (b) with intercalation only in the lower intercalation layer, and (c) with intercalation in both layers.

respectively. The calculation results show that Dy intercalation under the top layer graphene and under the buffer layer lowers the energy by 1.44 and 3.15 eV per Dy atom respectively with respect to the energy of 2×2 Dy adsorption on the top of graphene. The results clearly show that intercalation of Dy under the buffer layer is energetically quite favorable. We expect the lower intercalation layer to be filled first, followed by the upper layer intercalation. Our calculation also shows that the height (defined as the vertical distance from the top Si layer in the SiC substrate to the top of graphene layer) for the intercalation under the top graphene layer is 0.673 nm and that under the buffer layer is 0.794 nm. In comparison, this height is 0.880 nm when both carbon layers are intercalated. Therefore the height different between the double layer and top layer intercalation is 0.21 nm while that between the double layer and buffer layer intercalation is about 0.086 nm which is closer to the experimental measurement (see Figs. 2 and 3, and Fig. 6). Another evidence that excludes top layer intercalated graphene in contact with doubly intercalated graphene is the absence of $6\sqrt{3} \times 6\sqrt{3}$ on either side of the separating boundary as shown in Figs. 3 and 4 above. Occupation of the top layer will show attenuated $6\sqrt{3} \times 6\sqrt{3}$ since the buffer layer SiC interface is intact which is not observed experimentally.

We define the adsorption energy for a Dy atom on the (intercalated) epitaxial graphene as

$$E_{\mathrm{ad}} = E_{\mathrm{eg}} + E_{\mathrm{Dy,atom}} - E_{\mathrm{eg+Dy}}.$$

Here, E_{eg}, $E_{\mathrm{Dy,atom}}$, and $E_{\mathrm{eg+Dy}}$ are the energies of the (intercalated) epitaxial graphene without adsorption, the isolated Dy atom, and the whole system, respectively. It should be noted that $E_{\mathrm{Dy,atom}}$ corresponds to the energy of a Dy pseudoatom since we used a PAW potential of Dy that keeps the f electrons frozen in the core. Our calculation results for the adsorption energies are summarized in Table I. We note that the Dy adsorption energy is almost unaffected whether the lower intercalation layer is filled or not. However, we find that the additional intercalation in the upper intercalation layer (i.e., double-layer intercalation) enhances the stability of the adsorption by $\cong 0.82$ eV per atom. These results clearly indicate that bonding of Dy on graphene with Dy intercalated in both upper and lower carbon layers above the SiC(0001) substrate is much stronger. These results also suggest that the preferred Dy nucleation area observed in experiment as shown in Fig. 4 would correspond to the area with Dy intercalation in both upper and lower layers above the SiC substrate. In fact, the optimized atomic geometries obtained from the DFT calculations as shown in Fig. 6 also indicate that the difference in the vertical separation distances between the top graphene layer and the buffer carbon layer with and without Dy intercalation underneath the top graphene layer is about 0.086 nm, which is in excellent agreement with the height difference measured (with the correction due to different local work functions) from the STM experiment discussed in Sec. II.

TABLE I. Adsorption energy of Dy on the (intercalated) epitaxial graphene.

Configuration	$E_{\mathrm{ad}}^{\mathrm{Dy}}$ (eV)
No intercalation	1.55
Intercalation only in the lower intercalation layer	1.56
Intercalation in both upper and lower intercalation layer	2.38

We also investigate the electronic structures of the three structure models (before adsorption) shown in Fig. 5. The band structures obtained from our calculations are shown in Figs. 7(a)–7(f). For this system, the spin up and spin down are almost the same except for a flat band near the Fermi level in the spin up band for the nonintercalated structure [Fig. 7(a)] due to the dangling Si bonds at the surface of the SiC(0001) substrate. Once the buffer layer is intercalated with Dy, the Si dangling bonds are saturated and the band structure with spin up is identical to that of spin down as shown in Figs. 7(c), 7(d) and Figs. 7 (e), 7(f) respectively. We can see that without intercalation, the band structure exhibits a clear Dirac cone of single-layer graphene with slight n doping due to the effects of the SiC substrate and the buffer carbon layer which shift the Dirac point about 0.4 eV below the Fermi level as shown by the arrows in Figs. 7(a) and 7(b). This slightly n-doped behavior is well known in the literature [25]. When the carbon buffer layer is intercalated with Dy, it is decoupled from the SiC substrate and the system turns into bilayer graphene. Indeed, the band structure of the carbon layers shown in Figs. 7(c) and 7(d) exhibits the main features (i.e., a gap opening and parabolic dispersion as opposed to the linear one near the K point) of bilayer graphene under external electric field. We note that the Dirac point originated from the (decoupled) buffer layer lies about 1.5 eV below the Fermi level (as shown by the arrows) due to the electron transfer from the intercalated Dy layer. After both layers are intercalated with Dy, the band structure returns to that of (two decoupled) single layer graphene with the Dirac cones

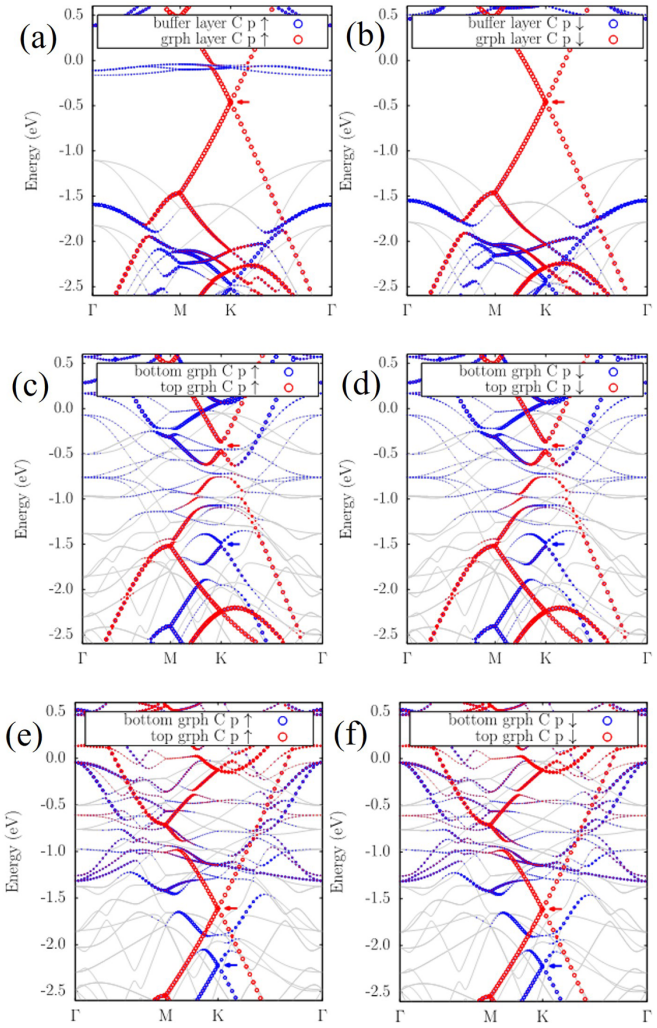

FIG. 7. Electronic band structures of the intercalated epitaxial graphene from DFT. The band structures are calculated for the epitaxial graphene (a) and (b) without intercalation, (c) and (d) with intercalation only in the lower intercalation layer, and (e) and (f) with intercalation in both intercalation layers. For each pair of figures, left and right figures are for spin up and down, respectively. Panel (e) was reproduced from the data used in Fig. 5(a) of Ref. [24]. Red and blue colors indicate the bands from the top graphene layer and the lower carbon layer, respectively. The size of the dots indicates the weight of the electronic state on the corresponding type of atoms. The gray lines represent the bands from other atoms.

heavily n doped and the Dirac points shift to 1.6 and 2.2 eV, respectively, below the Fermi level as shown by the arrows in Figs. 7(e) and 7(f). We note that the Dirac point of the top layer graphene in the double-layer intercalation case shown by the red arrow in Fig. 7(e) is about 1.0 eV lower than that of the buffer-layer intercalation case shown by the red arrow in Fig. 7(c). This result suggests that the work function in the buffer-layer intercalation structure would be higher than that of the double-layer intercalation structure, which is consistent with the experiment measurement discussed in the previous section. The different band structures due to different intercalation configurations from our first-principles calculations would be verified by future angular-resolved photoemission spectroscopy (ARPES) experiments.

It is interesting to note that adsorption and nucleation selectivity for Dy on single-intercalated versus double-intercalated graphene in the present study is different from what was observed in Ref. [8], where preferred nucleation of Eu and Cs in the nonintercalated graphene area on Ir(111) substrate has been observed. This difference can be attributed to the different substrate used. The electronic structure of Ir(111), the substrate used in Ref. [8], is very different from that of the SiC(0001) used in our system. Ir(111) is a close-packed metallic surface with the work function of ∼5.8 eV [26,27], which drives intense charge transfer from graphene to Ir and induces p doping [5,27]. The charge transfer in graphene-SiC(0001) is of opposite direction with resulting n doping. It is also worth noting that while the single layer graphene is directly on the top of Ir(111), there is a carbon buffer layer between the graphene layer and the Si-terminated SiC(0001) substrate in our system. Moreover, Eu and Cs metals used in Ref. [8] for intercalation and adsorption are highly electropositive mono- and divalent metals with a relatively lower work function of 2.0 and 2.5 eV as compared to the trivalent Dy with a work function of 3.3 eV [28] used in our present study. Therefore, details of the bonding mechanism of Cs, Eu, and Dy with the clean or intercalated graphene on Ir(111) and SiC(0001) would be very different.

To gain further insight into charge transform upon Dy adsorption in our system, we calculate the interaction charge density distribution caused by Dy adatom adsorption which is defined as the charge difference after and before the adatom adsorption, i.e., $\Delta\rho(\mathrm{r}) = \rho(\mathrm{r}) - [\rho_{\mathrm{gra/SiC}}(\mathrm{r}) + \rho_{\mathrm{adatom}}(\mathrm{r})]$ where $\rho(r)$ is the electron density of the whole sample including the adatom, $\rho_{\mathrm{gra/SiC}}(r)$ is the electron density of the system without adatom, and $\rho_{\mathrm{adatom}}(r)$ is the charge density of an isolated Dy adatom. $\rho_{\mathrm{gra/SiC}}(r)$ and $\rho_{\mathrm{adatom}}(r)$ are calculated using the same supercell conditions as those in the corresponding adsorption calculations. $\Delta\rho(r)$ accounts for the electron redistribution due to the interaction between the adatom and the rest of the system. The results of $\Delta\rho(r)$ in the four adsorption models are shown in Fig. 8. Positive values (red) in the plot indicate increases in the electron density after adsorption, and negative values (blue) indicate electron density reductions. Without intercalation, the interaction between the Dy adatom and the graphene is highly localized, causing the change in the electron density only in the vicinity of the adatom as can be seen from Fig. 8(a). When the top graphene layer or buffer carbon layer is intercalated, the interaction charge density $\Delta\rho(r)$ becomes conspicuous over both graphene layers and the intercalated Dy layer as in Figs. 8(b) and 8(c) respectively. Electrons in these layers are polarized upon the adsorption of Dy adatom. It is interesting to note that after both carbon layers are intercalated, the top carbon layer of the SiC substrate also becomes noticeably polarized as can be seen in Fig. 8(d). These results suggest that with Dy intercalation, the interaction between the Dy adatom and the substrate is far from being localized, and the response of the substrate also plays an important role in determining the energetic stability of the adsorption. Finally, we note that with the presence of SiC substrate, the electrons on the Dy adatom is also polarized notably in contrast to the

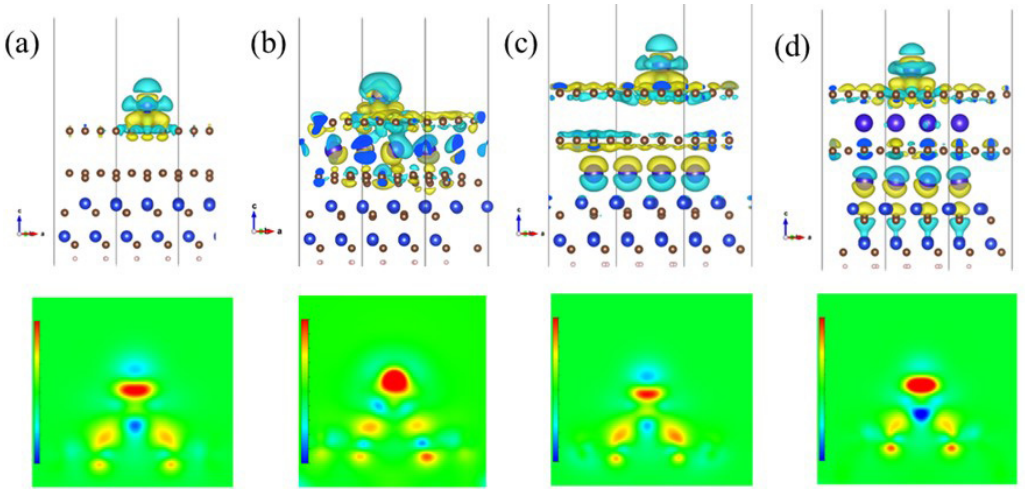

FIG. 8. Charge density differences in intercalated epitaxial graphene. The differences are depicted in the epitaxial graphene (a) without intercalation, (b) intercalation between the top graphene and buffer layer, (c) with lower-layer intercalation, and (d) with both-layer intercalation.

cases with Ir(111) substrate [8]. Moreover, the polarization of the electron in the Dy adatom is stronger when both carbon layers are intercalated.

IV. SUMMARY

In summary, using the atomic deposition technique and STM, we showed that Dy metal can be intercalated underneath the epitaxial graphene on Si-terminated SiC(0001) substrate. More interestingly, further deposition of Dy atoms exhibit strong preference for adsorption and nucleation in the Dy double-intercalated graphene rather than in the single-intercalated area. First-principles calculations showed that the adsorption energy for Dy on the graphene with Dy intercalated beneath both the graphene and the buffer carbon layer is about 0.82 eV larger than that without intercalation or with intercalation only under the buffer layer. This calculation result suggests that the areas with both the graphene layer and the buffer layer intercalated by Dy should have much higher Dy adsorption and nucleation probability than that in the area where only the buffer layer is intercalated. The prediction from the first-principles calculation is consistent with our experimental observation. Moreover, the difference in the interlayer distances and electronic band structures between SL intercalation and DL intercalation obtained from the first-principles calculations also agrees with experimental measurements.

ACKNOWLEDGMENTS

This work was supported by the U.S. Department of Energy, Office of Science, Basic Energy Sciences, Division of Materials Sciences and Engineering, including the computer time allocation at the National Energy Research Scientific Computing Center (NERSC) in Berkeley, CA. This work was performed at Ames Laboratory which is operated for the U.S. Department of Energy by Iowa State University under Contract No. DE-AC02-07CH11358.

[1] X. Liu, C.-Z. Wang, M. Hupalo, K.-M. Ho, H.-Q. Lin, and M. C. Tringides, Metals on graphene: Interactions, growth morphology, and thermal stability, Crystals **3**, 79 (2013).

[2] X. Liu, Y. Han, J. W. Evans, A. K. Engstfeld, R. Juergen Behm, M. C. Tringides, M. Hupalo, H.-Q. Lin, L. Huang, K.-M. Ho, D. Appy, P. A. Thiel, and C.-Z. Wang, Growth morphology and properties of metals on graphene, Prog. Surf. Sci. **90**, 397 (2015).

[3] K. V. Emtsev, A. A. Zakharov, C. Coletti, S. Forti, and U. Starke, Ambipolar doping in quasifree epitaxial graphene on SiC(0001) controlled by ge intercalation, Phys. Rev. B **84**, 125423 (2011).

[4] A. Sandin, T. Jayasekera, J. E. Rowe, K. W. Kim, M. Buongiorno Nardelli, and D. B. Dougherty, Multiple coexisting intercalation structures of sodium in epitaxial graphene-sic interfaces, Phys. Rev. B **85**, 125410 (2012).

[5] M. Petrovic, I. S. Rakic, S. Runte, C. Busse, J. T. Sadowski, P. Lazic, I. Pletikosic, Z. H. Pan, M. Milun, P. Pervan, N. Atodiresei, R. Brako, D. Sokcevic, T. Valla, T. Michely, and M. Kralj, The mechanism of caesium intercalation of graphene, Nat. Commun. **4**, 2772 (2013).

[6] J. Baringhaus, A. Stoehr, S. Forti, S. A. Krasnikov, A. A. Zakharov, U. Starke, and C. Tegenkamp, Bipolar gating of epitaxial graphene by intercalation of Ge, Appl. Phys. Lett. **104**, 261602 (2014).

[7] S. Schumacher, D. F. Forster, M. Rosner, T. O. Wehling, and T. Michely, Strain in Epitaxial Graphene Visualized by Intercalation, Phys. Rev. Lett. **110**, 086111 (2013).

[8] S. Schumacher, T. O. Wehling, P. Lazic, S. Runte, D. F. Foerster, C. Busse, M. Petrovic, M. Kralj, S. Bluegel, N. Atodiresei, V. Caciuc, and T. Michely, The backside of Graphene: Manipulating adsorption by intercalation, Nano Lett. **13**, 5013 (2013).

[9] Y. Cui, J. Gao, L. Jin, J. Zhao, D. Tan, Q. Fu, and X. Bao, An exchange intercalation mechanism for the formation of a two-

dimensional Si structure underneath graphene, Nano Res. **5**, 352 (2012).

[10] L. Jin, Q. Fu, R. Mu, D. Tan, and X. Bao, Pb intercalation underneath a graphene layer on Ru(0001) and its effect on graphene oxidation, Phys. Chem. Chem. Phys. **13**, 16655 (2011).

[11] A. Yurtsever, J. Onoda, T. Iimori, K. Niki, T. Miyamachi, M. Abe, S. Mizuno, S. Tanaka, F. Komori, and Y. Sugimoto, Effects of Pb intercalation on the structural and electronic properties of epitaxial graphene on SiC, Small **12**, 3956 (2016).

[12] D. McDougall, H. Hattab, M. T. Hershberger, M. Hupalo, M. Horn von Hoegen, P. A. Thiel, and M. C. Tringides, Dy uniform film morphologies on graphene studied with SPA-LEED and STM, Carbon **108**, 283 (2016).

[13] M. Hupalo, E. H. Conrad, and M. C. Tringides, Growth mechanism for epitaxial graphene on vicinal 6H-SiC(0001) surfaces: A scanning tunneling microscopy study, Phys. Rev. B **80**, 041401(R) (2009).

[14] P. Mallet, F. Varchon, C. Naud, L. Magaud, C. Berger, and J.-Y. Veuillen, Electron states of mono- and bilayer graphene on SiC probed by scanning-tunneling microscopy, Phys. Rev. B **76**, 041403(R) (2007).

[15] P. Lauffer, K. V. Emtsev, R. Graupner, T. Seyller, L. Ley, S. A. Reshanov, and H. B. Weber, Atomic and electronic structure of few-layer graphene on SiC(0001) studied with scanning tunneling microscopy and spectroscopy, Phys. Rev B **77**, 155426 (2008).

[16] L. Huang, Y. Wu, M. T. Hershberger, D. Mou, B. Schrunk, M. C. Tringides, M. Hupalo, and A. Kaminski, Effects of moiré lattice structure on electronic properties of graphene, Phys. Rev. B **96**, 035411 (2017).

[17] G. Binnig, H. Rohrer, Ch. Gerber, and E. Weibel, Surface Studies by Scanning Tunneling Microscopy, Phys. Rev. Lett. **49**, 57 (1982).

[18] N. D. Lang, Apparent barrier height in scanning tunneling microscopy, Phys. Rev. B **37**, 10395 (1988).

[19] G. Kresse and J. Hafner, *Ab initio* molecular dynamics for liquid metals, Phys. Rev. B **47**, 558(R) (1993).

[20] G. Kresse and J. Furthmüller, Efficient iterative schemes for *ab initio* total-energy calculations using a plane-wave basis set, Phys. Rev. B **54**, 11169 (1996).

[21] P. E. Blöchl, Projector augmented-wave method, Phys. Rev. B **50**, 17953 (1994).

[22] J. P. Perdew, K. Burke, and M. Ernzerhof, Generalized Gradient Approximation Made Simple, Phys. Rev. Lett. **77**, 3865 (1996).

[23] S. Grimme, J. Antony, S. Ehrlich, and H. Krieg, A consistent and accurate *ab initio* parametrization of density functional dispersion correction (DFT-D) for the 94 elements H-Pu, J. Chem. Phys. **132**, 154104 (2010).

[24] M. Kim, M. C. Tringides, M. T. Hershberger, S. Chen, M. Hupalo, P. A. Thiel, C.-Z. Wang, and K.-M. Ho, Manipulation of dirac cones in intercalated epitaxial graphene, Carbon **123**, 93 (2017).

[25] T. Ohta, A. Bostwick, J. L. McChesney, T. Seyller, K. Horn, and E. Rotenberg, Interlayer Interaction and Electronic Screening in Multilayer Graphene Investigated with Angle-Resolved Photoemission Spectroscopy, Phys. Rev. Lett. **98**, 206802 (2007).

[26] G. N. Derry, M. E. Kern, and E. H. Worth, Recommended values of clean metal surface work functions, J. Vac. Sci. Technol., A **33**, 060801 (2015).

[27] M. Kralj, I. Pletikosić, M. Petrović, P. Pervan, M. Milun, A. T. N'Diaye, C. Busse, T. Michely, J. Fujii, and I. Vobornik, Graphene on Ir(111) characterized by angle-resolved photoemission, Phys. Rev. B **84**, 075427 (2011).

[28] V. S. Fomenko, *Handbook of Thermionic Properties*, edited by G. V. Samsonov (Plenum, New York, 1966).